

TWO-VIEW EPIPOLE-BASED GUIDANCE CONTROL FOR AUTONOMOUS UNMANNED AERIAL VEHICLES

Achicanoy W.¹, Sagüés C.², López-Nicolás G.², and Rodríguez C.¹

¹*Departamento de Ingeniería Mecánica, Universidad de los Andes, Bogotá, Colombia*

²*Departamento de Informática e Ingeniería de Sistemas - Instituto de Investigación en Ingeniería de Aragón, Universidad de Zaragoza, María de Luna 1 E-50018, Zaragoza, España*
{wo.achicanoy115, crodrigu}@uniandes.edu.co, {csagues, gonlopez}@unizar.es

Keywords: UAV Guidance, Epipolar Geometry, Nonlinear Engagement, Input-Output Linearization, State Feedback.

Abstract: A vision-based control based on epipolar geometry is proposed to guide an autonomous unmanned aerial vehicle (UAV) to a target position. The interest of this contribution resides in a new and simple controller that allows purely vision-based guidance in a way that the accuracy of the system's state estimation, using sensors as Inertial Measurement Units (IMU) and Global Positioning Systems (GPS), is not critical. A current view and a target view are defined by a camera on-board the vehicle and a camera located at the target's position, respectively. The epipolar coordinates from these views are used to design a nonlinear control based on input-output linearization of the nonlinear engagement rule that relates the cameras' positions in the time. An integrator is included to force the outputs (epipolar coordinates) to follow an equilibrium point and a state feedback control law is proposed to stabilize the outcome of the linearized input-output mapping. Simulation experiments were done for the guidance of a small autonomous UAV that has a classical three-loop autopilot.

1 INTRODUCTION

Aerial unmanned vehicles (UAVs) are used in civilian and military applications developing tasks of surveillance and delivering cargo. Over the last decade, UAVs have proved to be efficient in several missions around the world, and the aircraft industry is working to improve the internal systems they have and to add new features and capabilities into the design. For example, vision system could enable UAVs tracking a large number of targets (Schneiderman, 2012). The UAV's performance commonly depends on aerial and ground operation centres and human assistance, but autonomous operation is necessary for stand-alone missions, or when the communication links fail and the vehicle needs to switch to a safe flight mode. The accuracy of the UAV's flight depends on the on-board sensors' capabilities and the control robustness it has; the navigation and guidance systems generally use Inertial Measurement Units (IMU) and Global Positioning Systems (GPS), to get information of the position and attitude; and cameras, spectrometers, and radars, to retrieve target's features, position and attitude. The cameras have been used in a wide range of applications for aerial, terrestrial, and aquatic vehicles (robots), and vision-based control has become

a special branch of research. Most of the research on vision-based control for autonomous UAVs have used the cameras' information, together with inertial and global positioning sensors, as inputs for filters or estimators. For example, a vision-based guidance based on trajectory optimization is proposed in (Watanabe et al., 2006) and the vision data is used for an EKF-filter to estimate the target's position and velocity relative to the vehicle. There, a cost function that minimizes the acceleration effort the vehicle demands to accomplish with three independent missions (target interception, obstacle avoidance, and formation flight) is included. In (Ma et al., 2007) a guidance law for a small UAV is developed based on an adaptive filter that calculates the target's velocity over the image plane. The filter only uses the tracking information of the moving target and a control regulates the vehicle's yaw rate at a constant altitude (no depth information is required).

From another point of view, visual-based control methods based on epipolar geometry and homography have been used for mobile robot navigation. (Mariottini et al., 2004) and (López-Nicolás et al., 2008) have developed two-view visual-control for nonholonomic robots by means of nonlinear control and tracking of epipoles signals. In (López-Nicolás

et al., 2010) both epipolar geometry and homography matrix are used to design separated controls that are switched by the degeneracy of the fundamental matrix (ill-conditioned). Epipole-based control is used at the initial stage of the navigation, whereas homography-based control is used at the end (short baseline). Separately, homography has been used for UAV navigation. In (Hu et al., 2007b) a multi-view visual-based control, that uses quaternions and homography between pre-recorded satellite images and vehicle's actual images, is proposed to track a desired trajectory over the earth. Given that the estimated position is up to scale and the depth is unknown, open problems in this approach are clarified in (Hu et al., 2007a). In (Kaiser et al., 2010) a multi-view visual-based estimator based on homography and GPS measurements is designed, and an autopilot commands the vehicle's control surfaces. The continuous tracking of features, entering and leaving the vehicle's camera Field of View (FoV), and the GPS failures (past measurements are used when it fails) are the main challenges this estimator deals with.

In this paper, given that the epipolar geometry has reported successful outcomes in mobile robots, a new and simple controller based on epipolar geometry for guidance of an autonomous UAVs with a single camera on-board is developed (sensor fusion is not considered). A vertical planar motion is assumed and two views, the current view (vehicle's camera) and the target view (static camera at the target's position), are used to compute the epipoles and to steer the vehicle to a desired position. As in (Mariottini et al., 2004) and (López-Nicolás et al., 2008), input-output linearization (Khalil, 2002) is used but over the cameras' nonlinear engagement rule. The linearized output is stabilized by an appropriated state feedback control law and the outputs (epipolar coordinates) are forced to follow an equilibrium point by means of an integrator, that eliminates the steady state error and improves the robustness of the closed-loop system. Both epipolar coordinates in the current and target views are independently chosen as outputs. Also, to deal with the complexity of the aerial models (due to nonlinear aerodynamics) a classical three-loop autopilot (Zarchan, 2007) is used. The controller reduces the complexity of the on-board electronics the vehicle needs to transport, and the fact that only epipolar estimation is required, makes it suitable for simple guidance applications. The paper is organized as follows: in section 2 the planar epipolar geometry is shown; in section 3 a state space representation of the nonlinear planar engagement rule is done; in section 4 the control strategy is developed; and in section 5 results of the simulation experiments are analysed.

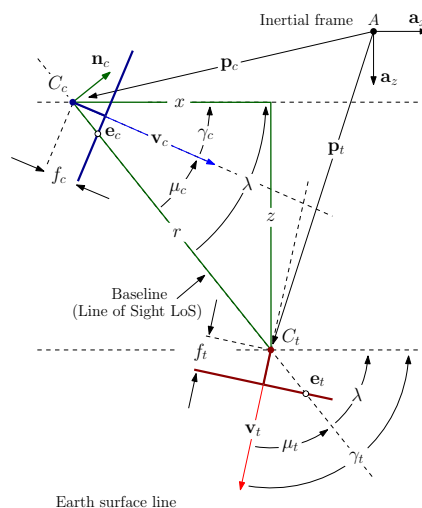


Figure 1: Planar two-view epipolar geometry (plane xz).

2 PLANAR EPIPOLAR GEOMETRY

Figure 1 shows the planar two-view epipolar geometry, relative to the inertial reference frame A , for the autonomous UAV guidance problem. The first view is defined by a current camera C_c on-board the vehicle, that is aligned to a current velocity vector $\mathbf{v}_c = [u_c^A, w_c^A]^T$ and located at a current position $\mathbf{p}_c = [x_c^A, z_c^A]^T$, while the second view is an image previously defined by a target camera C_t , that is aligned to a target velocity $\mathbf{v}_t = [u_t^A, w_t^A]^T$ at a position $\mathbf{p}_t = [x_t^A, z_t^A]^T$. The epipoles (in pixel) $\mathbf{e}_c \in \mathbb{R}^2$ (current) and $\mathbf{e}_t \in \mathbb{R}^2$ (target) are subject to the constraints $F\mathbf{e}_c = \mathbf{0}$ and $F^T\mathbf{e}_t = \mathbf{0}$, where $F \in \mathbb{R}^{3 \times 3}$ is the fundamental matrix. F is usually estimated from a set of features correspondences by means of a robust algorithm as the Random Sample Consensus (RANSAC) (Hartley and Zisserman, 2004). These epipoles can be written as $\mathbf{e}_c = [e_{c,w}, e_{c,h}]^T$ and $\mathbf{e}_t = [e_{t,w}, e_{t,h}]^T$, respectively, where $(e_{c,w}, e_{t,w})$ and $(e_{c,h}, e_{t,h})$ are the coordinates along the image's width and height, respectively. For planar guidance design only the coordinates $(e_{c,h}, e_{t,h})$ are useful, and according to the Fig. 1, it follows that

$$e_{c,h} = f_c \tan(\lambda - \gamma_c) \quad (1a)$$

$$e_{t,h} = -f_t \tan(\gamma_t - \lambda), \quad (1b)$$

where f_c and f_t (in pixel) are the focal lengths for the current camera and the target camera, respectively; λ is the Line of Sight (LoS) angle, that is measured between the LoS and the \mathbf{a}_x -axis; and γ_c and γ_t are the flight path angles for the current camera and the target camera, respectively. These angles are measured between the velocity vectors \mathbf{v}_c and \mathbf{v}_t and the \mathbf{a}_x -axis. By definition the baseline is equal to the LoS.

3 PLANAR ENGAGEMENT RULE

The planar engagement rule is a description of the evolution of the LoS angle λ and the LoS rate of change $\dot{\lambda}$ according to a lateral acceleration command \mathbf{n}_c . If \mathbf{n}_c is proportional to $\dot{\lambda}$, then, the current camera C_c (vehicle) can be steered to the target camera C_t (target); this is the intuitive Proportional Navigation (PN) (Yanushevsky, 2007). From the Fig. 1, it is obtained that $\lambda = \arctan(z/x)$, where $x = x_t^A - x_c^A$ and $z = z_t^A - z_c^A$, and the LoS rate of change is

$$\dot{\lambda} = \frac{\dot{z}x - z\dot{x}}{r^2}, \quad (2)$$

where $r = \sqrt{x^2 + z^2}$ is the magnitude of the instantaneous separation (range) between C_c and C_t . If (2) is differentiated again, and taking into account that $\cos(\lambda) = x/r$ and $\sin(\lambda) = z/r$, it follows that

$$\ddot{\lambda} = \frac{\ddot{z}\cos\lambda - \dot{z}\sin\lambda}{r} - \frac{2\dot{r}\dot{z}\cos\lambda + 2\dot{r}\dot{x}\sin\lambda}{r^2}. \quad (3)$$

Given that C_t is static, the C_c 's acceleration components, in terms of the lateral acceleration magnitude n_c , are $\ddot{x} = -n_c \sin\lambda$ and $\ddot{z} = n_c \cos\lambda$, then, (3) can be simplified as

$$\ddot{\lambda} = \omega \sin(\lambda - \phi) + n_c/r, \quad (4)$$

where $\omega = 2(v_{cl}/r)^2$ and $\phi = \arctan(\dot{z}/\dot{x})$. $\mathbf{v}_{cl} = -\dot{\mathbf{r}}$ is commonly known as the closing velocity. Finally, the planar engagement can be presented as the continuous nonlinear system

$$\dot{\eta} = f(\eta, u) = \begin{bmatrix} \eta_2 \\ \omega \sin(\eta_1 - \phi) + u/r \end{bmatrix}, \quad (5)$$

where $\eta = [\eta_1, \eta_2]^T = [\lambda, \dot{\lambda}]^T \in \mathbb{R}^2$ is the state vector, $u = n_c \in \mathbb{R}$ is the input, and $f(\eta, u) : \mathbb{R}^2 \times \mathbb{R} \rightarrow \mathbb{R}^2$ is a vector field.

4 EPIPOLE-BASED GUIDANCE CONTROL

A guidance control based on input-output linearization (Khalil, 2002) of the engagement system (5), with output based on the epipolar coordinates' measurements from the two views, and a control law based on state feedback, that includes integral action, are developed. Both the coordinate $e_{c,h}$, defined by the Eq. (1a), and the coordinate $e_{t,h}$, defined by the Eq. (1b), are used independently as outputs, i.e., $y = e_{c,h}$ or $y = e_{t,h}$. If y is differentiated until the input u becomes explicit, and taking into account the

system (5), then, it results that the relative degree the system has is 2, for all $\eta \in \mathbb{R}^2$, and the controls

$$u = -r\omega \sin(\eta_1 - \phi) - 2r(\eta_2 - \dot{\gamma}_c)^2 \tan(\eta_1 - \gamma_c) + r\ddot{\gamma}_c + \left[r \cos(\eta_1 - \gamma_c)^2 / f_t \right] v \quad (6)$$

or

$$u = -r\omega \sin(\eta_1 - \phi) + 2r\eta_2^2 \tan(\gamma_t - \eta_1) + \left[r \cos(\gamma_t - \eta_1)^2 / f_t \right] v, \quad (7)$$

for $y = e_{c,h}$ and $y = e_{t,h}$, respectively, lead the nonlinear output to the linearized mapping

$$\begin{aligned} \dot{\xi}_1 &= \xi_2 \\ \dot{\xi}_2 &= v \\ \sigma &= e, \end{aligned} \quad (8)$$

where $\xi_1 = y$, $\xi_2 = \dot{y}$, and v is the new control. An integral action was included in (8) forcing the output y to follow a reference $\xi_1^r = y^r$. $e = \xi_1 - \xi_1^r = y - y^r$ is the output error. It is easily verified that the augmented system (8) with realization

$$A_a = \begin{bmatrix} 0 & 1 & 0 \\ 0 & 0 & 0 \\ 1 & 0 & 0 \end{bmatrix} \quad B_a = \begin{bmatrix} 0 \\ 1 \\ 0 \end{bmatrix} \quad C_a = [1 \quad 0 \quad 0] \quad (9)$$

has a controllable pair (A_a, B_a) , and a state feedback control

$$v = -\mathbf{K}[\xi, \sigma]^T, \quad (10)$$

where $\mathbf{K} = [k_1, k_2, k_3]$, can stabilize it. \mathbf{K} is chosen such that the matrix $(A_a - B_a \mathbf{K})$ is Hurwitz (pole placement) (Khalil, 2002) and local stability is guaranteed.

5 SIMULATION EXPERIMENTS AND ANALYSIS

Figure 2 shows the model of an UAV, without propulsion and with a camera on-board, that was designed and implemented to evaluate the guidance control. For simplicity, a wing-body-tail configuration with a horizontal control surface (wing) and a stabilizing fixed surface (tail) was selected. Fast control is guaranteed by means of the wing's deflection angle δ , even though nonlinearities and rear stability interferences might appear on it (Chin, 1961). Given that the down-range is limited, the earth is assumed to be flat. Three

reference frames are defined: (i) The inertial A (located at an initial altitude h_0); (ii) the vehicle-fixed B (aligned to the principal axes); and (iii) the camera-fixed C (aligned to the vehicle's velocity vector \mathbf{v} or aero-stabilized). The camera's principal axis is parallel to \mathbf{c}_x -axis. The camera usually is in the apex of the nose, but for simplicity, it is assumed that it is at the cg . Rotation and translation equations can be found in (Siouris, 2004), and the estimation of the aerodynamic coefficients was done with the Vortex Lattice Method (VLM) (Melin, 2000). The drag, lift and pitch coefficients, that for simplicity, only depend on the scheduling variables h (altitude) and M (Mach number), are stored in look-up tables. Also, a classical three-loop autopilot (gyro and acceleration feedback), that translates acceleration commands u to wing deflections δ is chosen. A complete description of the autopilot and the design equations can be found in (Zarchan, 2007). The Fig. 3 shows the autopilot outputs for the unitary step acceleration command $u = u_s(t-1)G$ (u_s is the unitary step function) and for the flight conditions $h = 0$ m (black continuous lines), $h = 1000$ m (red dotted lines), $M = 0.3$, and $M = 0.9$. For simplicity, the actuator's dynamics are neglected and ideal sensors are assumed. The design parameters are $\omega_{CR} = 50$ rad/s (crossover frequency measured at the gain margin), $\zeta = 0.7$ (total acceleration damping), and $\tau = 0.2$ s (total acceleration time constant). The Fig. 3(a) and the Fig. 3(d) show the agreement between the desired acceleration output n and the design parameters. It is noted that the vehicle's high manoeuvrability is reached at low altitude h and high Mach number M , and the angle of attack α and the deflection angle δ stay at low values (Fig. 3(e) and Fig. 3(f), respectively). For $M \leq 0.3$ the autopilot demands high values of α and δ (Fig. 3(b) and Fig. 3(c), respectively), and the actuator's limits and the vehicle's aerodynamics capabilities are exceeded. This flight condition can lead the system to instability. Due that the vehicle's parameters change with the flight conditions, a look-up table (with linear interpolation) is implemented to change the autopilot gains according to the values of h and M .

On the other hand, for the simulations, it is assumed that the cameras C_c and C_t are equal, ideal (skew factor is zero) and finite (Hartley and Zisserman, 2004). The image resolution is 480×640 pixels (height x width), the focal length is $f = f_c = f_t = 240$ pixel, and the epipoles' measurements are assumed to be known only from geometric relationships. The frame A is fixed at the initial altitude $h_0 = 2500$ m, the vehicle's initial velocity is $\mathbf{v}_0 = 200\mathbf{b}_x$ m/s, and the initial attitude angle θ is equal to the current camera C_c 's attitude angle γ_c , i.e., the initial angle of attack

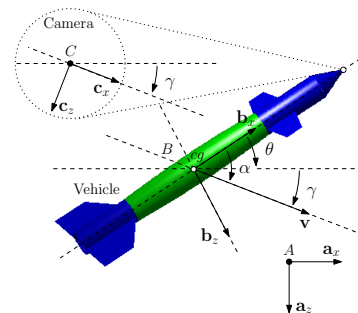


Figure 2: Autonomous UAV. Reference frames in the vertical plane xz are: A (inertial), B (vehicle-fixed), and C (camera-fixed).

$\alpha_0 = 0$ deg. The state feedback control gain \mathbf{K} is calculated with the Acker's formula. Initially, it is shown that the control with unforced output y , for both control based on $y = e_{t,h}$ and control based on $y = e_{c,h}$, can be considered as PN-based control. This fact can be explained by means of the differentiation of the Eq. (1b), that results in a directly proportional relationship between the rate of change of the target epipolar coordinate $\dot{e}_{t,h}$ and the LOS rate of change $\dot{\lambda}$. As in PN, the feedback of $\dot{e}_{t,h}$ times an appropriate constant can stabilize the linearized output (8), which means that the LoS angle λ is constant and the control based on $y = e_{t,h}$ can steer the vehicle to the target position (parallel navigation). An exact estimation of \mathbf{v}_{cl} is not necessary, furthermore, if the vehicle's path angle γ_c is replaced by a constant value, then, the differentiation of the Eq. (1a) results in a directly proportional relationship between $\dot{e}_{c,h}$ and $\dot{\lambda}$, and the control based on $y = e_{c,h}$ is able to steer the vehicle to the target position too. The Fig. 4 shows the outputs of both control based on $y = e_{t,h}$ and control based on $y = e_{c,h}$ for a set of current cameras $C_{c,1}$ at $\mathbf{p}_{c,1} = [0, 0]^T$ m, $C_{c,2}$ at $\mathbf{p}_{c,2} = [500, 0]^T$ m, and $C_{c,3}$ at $\mathbf{p}_{c,3} = [1000, 0]^T$ m. The initial attitude angle is $\theta_0 = 45$ deg for all the cameras. The Fig. 4(a) and the Fig. 4(d) show that all cameras converge to the target camera C_t at $\mathbf{p}_t = [2000, 2000]^T$ m ($\gamma_t = 90$ deg) for $y = e_{t,h}$ and $y = e_{c,h}$, respectively. Feedback gain K is equal for both controls. The arrows show the initial and final attitudes for the current cameras (attitude control is not done by the controls). Differences between the two guidance controls are noted, mainly, in the shape of the trajectories. The Fig. 4(b) and the Fig. 4(f) show that the epipolar coordinates reach equilibrium points of $e_{t,h}$ and $e_{c,h}$ for the controls based on $y = e_{t,h}$ and $y = e_{c,h}$, respectively. The Fig. 4(c) and the Fig. 4(e) show the free evolution of $e_{c,h}$ and $e_{t,h}$ for the controls based on $y = e_{t,h}$ and $y = e_{c,h}$, respectively. The shape

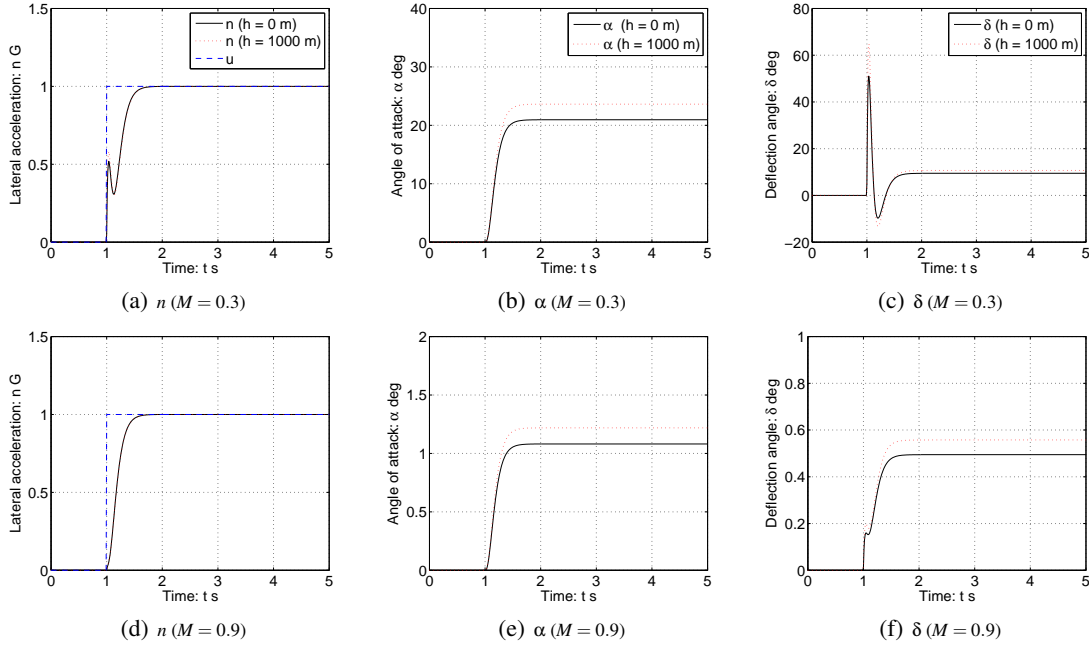


Figure 3: Autopilot response to step input $u = u_s(t - 1)$ G (blue dashed lines) at altitudes $h = 0$ m (black continuous lines) and $h = 1000$ m (red dotted lines). The first and second rows show the outputs for the Mach numbers $M = 0.3$ and $M = 0.9$, respectively.

of the vehicle's trajectory is defined by the shape of the output epipolar coordinates. The Fig. 5(a) and the Fig. 5(d) show the control u (command acceleration required for the three cameras $C_{c,1}$, $C_{c,2}$, and $C_{c,3}$), for the controls based on $y = e_{t,h}$ and $y = e_{c,h}$, respectively. At the initial stage of the guidance maximum acceleration effort is required for both controls, however, the control based on the coordinate $e_{c,h}$ requires more acceleration than the control based on the coordinate $e_{t,h}$. Control based on $e_{t,h}$ does not develop high oscillations at the initial stage of the guidance, but it needs high values of α and δ . The Fig. 5(b) and the Fig. 5(e) show the angle of attack α , and the Fig. 5(c) and the Fig. 5(f) show the deflection angle δ , for the control based on $y = e_{t,h}$ and the control based on $y = e_{c,h}$, respectively. After the initial stage of the guidance, the values of the angles α and δ required for the control based on $y = e_{c,h}$ are small than the values required for the control based on $e_{t,h}$. The camera $C_{c,3}$ requires the higher values of u , α and δ , due to the initial condition it has (it is ahead of the other cameras and needs more turn effort).

Next, the outputs $y = e_{t,h}$ and $y = e_{c,h}$, are forced to follow an equilibrium reference. The Fig. 6(a) and The Fig. 6(b) show the outputs of the controls based on $y = e_{t,h}$ and $y = e_{c,h}$ for the reference signals $e_{t,h}^r = e_{c,h}^r = -10k$ pixel, for $kT \leq t < (k+1)T$, $k = 0, 1, 2, \dots$, $T = 4$ s, and $t \geq 0$. The initial current camera C_c is located at $\mathbf{p}_c = [0, 0]^T$ m with initial atti-

tude angle $\theta_0 = 45$ deg. The target camera C_t is fixed at $\mathbf{p}_t = [2000, 2000]^T$ m and aligned to C_c with attitude angle $\gamma_t = 45$ deg. The gain \mathbf{K} has the same value for both controls. It is noted that the epipolar coordinates follow the equilibrium points for both $y = e_{t,h}$ and $y = e_{c,h}$. As in the previous simulation, it is noted that at the initial stage of the guidance, the control based on $y = e_{c,h}$ requires more acceleration effort than the control based on $e_{c,h}$. After this stage, small values of α (compare the Fig. 6(b) and the Fig. 6(e)) and δ (compare the Fig. 6(c) and the Fig. 6(f)) are required for the control based on $y = e_{c,h}$. The fact that both outputs can follow a reference allows the controls to guide the vehicle with a reference LoS angle λ to the target camera position (λ is directly related to the epipolar trajectories) and a limited control of attitude can be achieved (it is limited due to the vehicle's aerodynamics). The attitude control and tracking of reference signals are proposed as future work. In addition, a reduction of the autopilot's gain margin (stability) is noted and the total damping and time response are affected (see the settling time in the Fig. 6(a) and the Fig. 6(b)). A re-design of the autopilot and the adjustment of the gain vector \mathbf{K} are done, taking into account that k_1 is related to the total damping, k_2 is related to the LoS rate $\dot{\lambda}$ stabilization, and k_3 is related to the integral action and the oscillations that would appear in the outputs. The above simulation was done with $\omega_{CR} = 10$ rad/s, $\zeta = 0.7$, $\tau = 0.2$ s, and

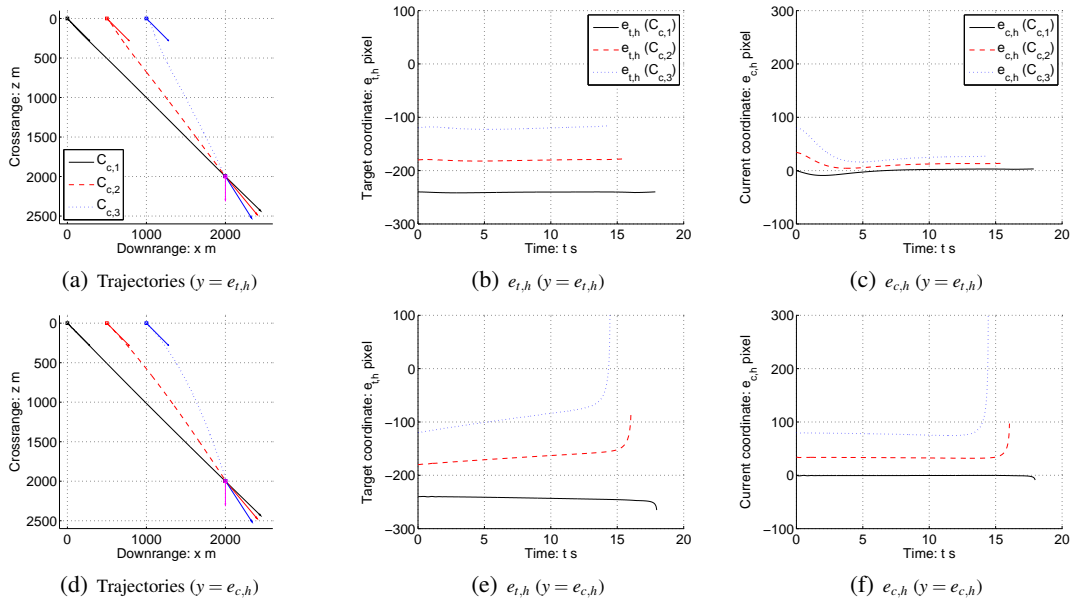


Figure 4: Outputs of the guidance based on both output $y = e_{t,h}$ and output $y = e_{c,h}$ for the three current cameras $C_{c,1}$, $C_{c,2}$, and $C_{c,3}$, positioned at different space locations but with the same initial attitude angle $\theta_0 = 45$ deg. The first and second rows show the outputs for $y = e_{t,h}$ and $y = e_{c,h}$, respectively.

$\mathbf{K} = [8, 2, 8]$. In the other hand, the initial stage of the guidance is the worse flight condition that the autopilot has to deal, high altitude h and low Match number M make the autopilot requires high values of angles α and δ . This initial condition affects more the control based on $e_{c,h}$ than the control based on $e_{t,h}$. One way to improve the initial response of the autopilot is to rise the value of the vehicle's initial velocity, but it is constrained to the aerodynamic limits of the aircraft that launches it.

6 CONCLUSIONS

A epipole-based control has been developed to control the guidance of an autonomous UAV. Only epipolar measurements from two views were used to steer the vehicle to a static camera position. Stabilizing of a nonlinear engagement rule by an input-output nonlinear control strategy was developed and two different alternatives of guidance, based on current epipolar coordinate and based on target epipolar coordinate, were studied. Also, an integral action guarantees the epipolar coordinates follow a reference equilibrium point. A model of a small UAV, that includes a classical three-loop autopilot, was used to simulate the control strategies. For future work a combination of these alternatives of control, tracking of reference signals and stability analysis are proposed.

ACKNOWLEDGEMENTS

This work was supported by Universidad de los Andes, Ministerio de Ciencia e Innovación / Unión Europea DPI2009-08126, and Universidad de Nariño.

REFERENCES

- Chin, S. (1961). *Missile configuration design*. McGraw-Hill, 1st edition.
- Hartley, R. I. and Zisserman, A. (2004). *Multiple View Geometry in Computer Vision*. Cambridge University Press, ISBN: 0521540518, 2nd edition.
- Hu, G., Gans, N., Mehta, S., and Dixon, W. (2007a). Daisy chaining based visual servo control part ii: Extensions, applications and open problems. In *Control Applications, 2007. CCA 2007. IEEE International Conference on*, pages 729 – 734.
- Hu, G., Mehta, S., Gans, N., and Dixon, W. (2007b). Daisy chaining based visual servo control part i: Adaptive quaternion-based tracking control. In *Control Applications, 2007. CCA 2007. IEEE International Conference on*, pages 1474 – 1479.
- Kaiser, M. K., Gans, N. R., and Dixon, W. E. (2010). Vision-based estimation for guidance, navigation, and control of an aerial vehicle. *Aerospace and Electronic Systems, IEEE Transactions on*, 46(3):1064 – 1077.
- Khalil, H. K. (2002). *Nonlinear Systems*. Prentice Hall, ISBN: 0130673897, 3rd edition.
- López-Nicolás, G., Guerrero, J., and Sagüés, C. (2010).

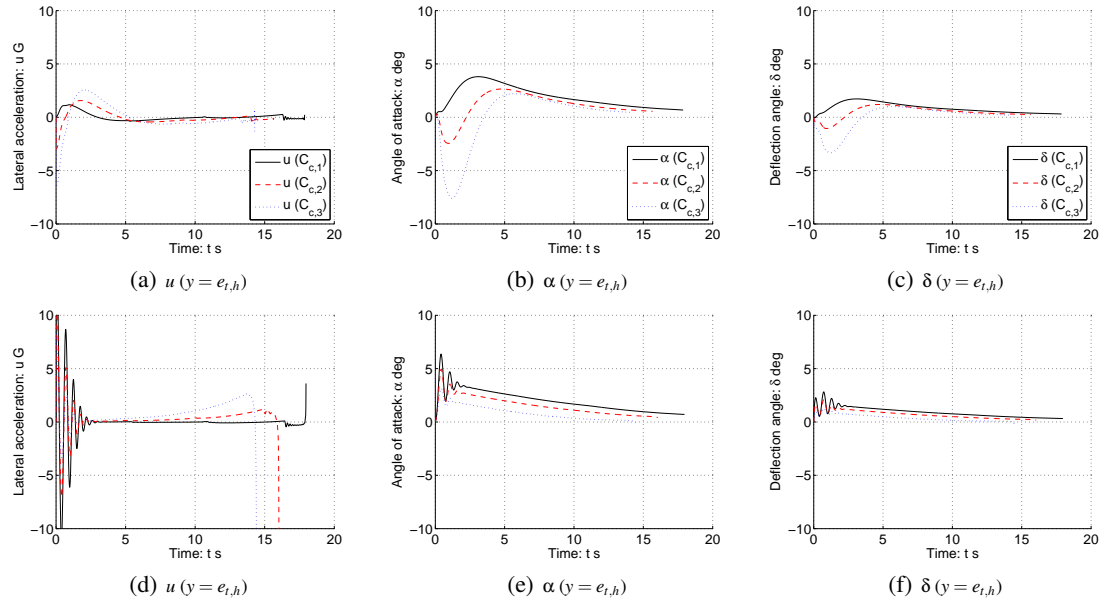


Figure 5: Control input u , angle of attack α , and deflection angle δ for the set of current cameras $C_{c,1}$, $C_{c,2}$, and $C_{c,3}$. The first and the second rows correspond to the controls based on $y = e_{t,h}$ and $y = e_{c,h}$, respectively.

Visual control of vehicles using two-view geometry. *Mechatronics*, 20(2):315 – 325.

- López-Nicolás, G., Sagüés, C., Guerrero, J., Kragic, D., and Jensfelt, P. (2008). Switching visual control based on epipoles for mobile robots. *Robotics and Autonomous Systems*, 56(7):592 – 603.
- Ma, L., Cao, C., Hovakimyan, N., and Woolsey, C. (2007). Development of a vision-based guidance law for tracking a moving target. In *AIAA Guidance, Navigation and Control Conference and Exhibit*. AIAA.
- Mariottini, G., Prattichizzo, D., and Oriolo, G. (2004). Epipole-based visual servoing for nonholonomic mobile robots. In *Robotics and Automation, 2004. Proceedings. ICRA '04. 2004 IEEE International Conference on*, volume 1, pages 497 – 503.
- Melin, T. (2000). A vortex lattice matlab implementation for linear aerodynamic wing applications. Master's thesis, Royal Institute of Technology (KTH).
- Schneiderman, R. (2012). Unmanned drones are flying high in the military/aerospace sector [special reports]. *Signal Processing Magazine, IEEE*, 29(1):8 – 11.
- Siouris, G. M. (2004). *Missile Guidance and Control Systems*. Springer New York, ISBN: 9780387007267, 1st edition.
- Watanabe, Y., Johnson, E., and Calise, A. (2006). Vision-based guidance design from sensor trajectory optimization. In *AIAA Guidance, Navigation and Control Conference and Exhibit*. AIAA.
- Yanushevsky, R. (2007). *Modern Missile Guidance*. CRC Press, ISBN: 1420062263, 1st edition.
- Zarchan, P. (2007). *Tactical and Strategic Missile Guidance*. American Institute of Aeronautics and Astronautics Inc., ISBN: 9781563478741, 5th edition.

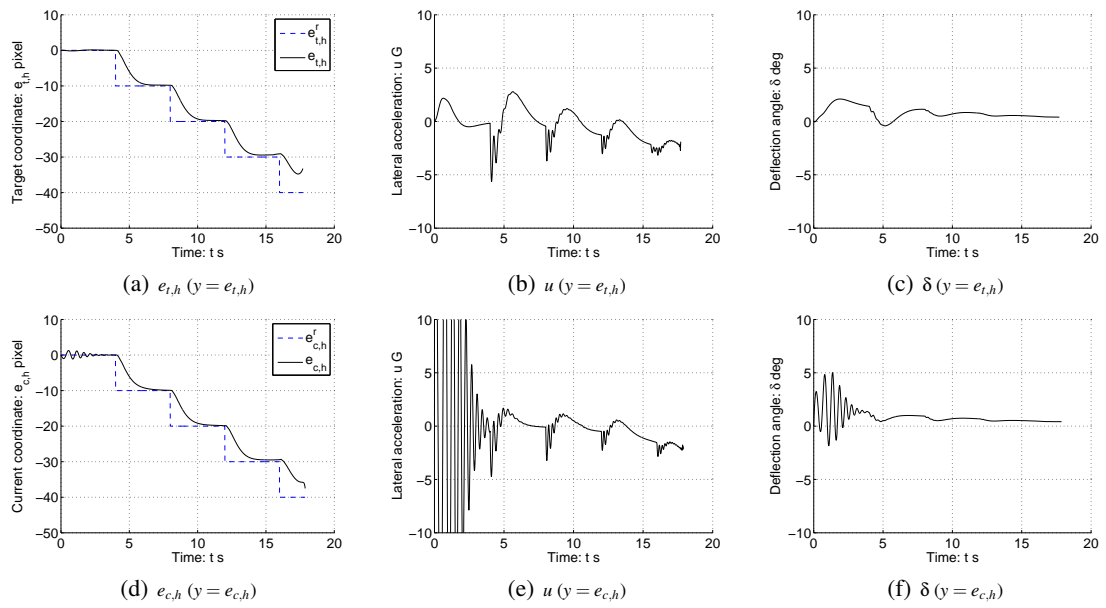


Figure 6: Epipolar coordinates for the reference signals $e_{t,h}^r = e_{c,h}^r = -10k$, for $kT \leq t < (k+1)T$, $k = 0, 1, 2, \dots$, $T = 4$ s, and $t \geq 0$; control input u ; and deflection angle δ . Target camera C_t is fixed at $\mathbf{p}_t = [2000, 2000]^T$ m and aligned to C_c with attitude angle $\gamma_t = 45$ deg. The first and second rows correspond to the controls based on $y = e_{t,h}$ and $y = e_{c,h}$, respectively.